DØ Note 5454-CONF

Search for Long-lived Particles Decaying into Z bosons

The DØ Collaboration
URL http://www-d0.fnal.gov
(Dated: August 6, 2007)

We present a search for heavy long-lived particles decaying into a Z boson in appoximately 1.1 fb^{-1} of DØ data accumulated during Run IIa. Such particles can be present in some models with gauge-mediated supersymmetry breaking, hidden valley models, an extended Higgs sector, and in models with a fourth generation quark. We use pointing of the electromagnetic showers in DØ calorimeter and preshower systems to search for displaced vertices and look for excess of vertices at a large distance from the beam. No evidence of such excess is found, and we set limits on the production cross-section and lifetime of long-lived particles, using fourth generation quark as a benchmark model.

Preliminary Results for Summer 2007 Conferences

I. INTRODUCTION

The success of the standard model (SM) has been quite unexpected, given its shortcomings. The number of free parameters ranging over many orders of magnitude, absence of dark matter candidates, the hierarchy problem, lack of gauge coupling unification, and no path to incorporate gravity naturally lead to the belief that the SM is but a low-energy approximation of some more general and aesthetically pleasing theory. Yet despite all efforts no significant deviations from the SM predictions have been found to date.

In this note we present a search for a signature that has not been studied as thoroughly as many others, namely a signature of long-lived particles that travel tens of centimeters before decaying into a Z boson which we detect in the di-electron decay mode. There are many models that predict existence of such long-lived particles: supersymmetry (SUSY) with gauge mediation [1, 2], hidden valley models [3], models with an extended Higgs sector [4], and fourth generation quark (b') [5] to name a few. A couple of typical Feynman diagrams are shown in Fig. 1.

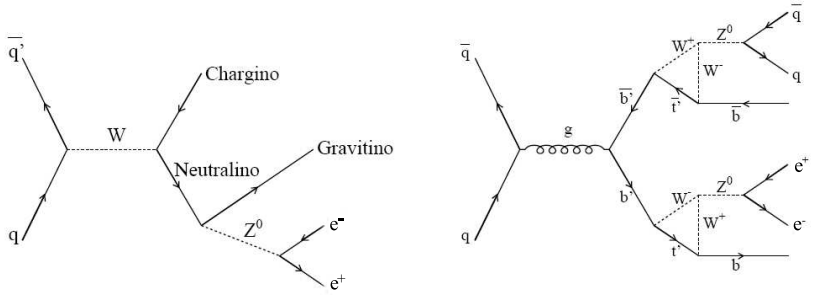

FIG. 1: Typical sources of Z boson production away from primary vertex: GMSB SUSY (left) and long-lived b'(right).

The CDF collaboration reported a search for such particles using Z boson decays to muons and reconstructing di-muon vertices in the tracker [6]. Sensitivity to long lifetimes in the CDF analysis is limited by tracking and trigger efficiency for muons with large impact parameters. For this analysis we used the capability of DØ detector to reconstruct the direction of electro-magnetic (EM) showers, which allows us to be be sensitive to much longer lifetimes.

Although we set limits within the framework of the b' model, we were careful not to impose potentially model-dependent selection requirements. For example, we require a very loose dielectron mass requirement (greater than 75 GeV), to remain sensitive to new particles that are heavier than a Z boson and that decay into electrons or photons.

II. DETECTOR DESCRIPTION

The data used in this analysis were recorded by the DØ detector [7]. The DØ detector utilizes a right-handed coordinate system with the z-coordinate aligned with the beam-line, x-axis directed horizontally away from the center of the accelerator ring, and y-axis directed upwards. The azimuthal angle ϕ of a point with coordinates (x, y, z) is defined in the transverse, xy plane with respect to x axis. The longitudinal, rz plane is defined by radius vector r defined as $r \equiv \sqrt{x^2+y^2+z^2}$. The pseudorapidity of this point is $\eta = -\log(\tan(\theta/2))$, where $\theta = \arctan(sqrt(x^2+y^2)/z)$. The spatial separation between two objects in the detector is defined as $\Delta\mathcal{R} \equiv \sqrt{\delta\phi^2+\delta\eta^2}$, where $\delta\phi$ and $\delta\eta$ are separation between the objects in azimuthal angle and pseudorapidity, respectively.

The DØ detector has a central-tracking system, consisting of a silicon microstrip tracker (SMT) and a central fiber tracker (CFT), with designs optimized for tracking and vertexing at pseudorapidities $|\eta| < 3$ and $|\eta| < 2.5$, respectively. These tracking detectors are located within a 2 T superconducting solenoidal magnet. A liquid-argon and uranium calorimeter has a central section (CC) covering pseudorapidities $|\eta|$ up to 1.2, and two end calorimeters that extend coverage to $|\eta| \approx 4.2$ with all three housed in separate cryostats [8]. The electromagnetic (EM) section of the calorimeter has four longitudinal layers and transverse segmentation of 0.1×0.1 in $\eta - \phi$ space, except in the third layer, where it is 0.05×0.05. The central preshower system (CPS) provides precision position measurements for EM showers with $|\eta| < 1.2$.

M(b'), GeV	Number of events expected in 1.1 fb^{-1}	Cross-section, pb
100	548±82	79.0
130	154±23	23.5
150	58±9	11.8
160	53±8	8.6
170	28±4	6.4
180	21±3	4.8
190	20±3	3.6

TABLE I: Masses, expected number of signal events in 1.1 fb^{-1}, and pair-production cross-sections for b' events generated with $c\tau$=100 mm.

III. SIGNAL SIMULATION

We used PYTHIA v 6.202 [9] to generate the events with pair-produced b' quarks. We assumed that all b' quarks decay into a Z boson and a b-quark. We then select events that have at least one of the two Z bosons in the final state decaying into e^+e^-, and put them through a full detector simulation and reconstruction chain. We generated b' masses between 100 and 190 GeV and lifetimes ($c\tau$) between 1 and 9000 mm. The cross-sections and expected number of events for b' with $c\tau$=100 mm is given in Table I.

IV. EM OBJECT IDENTIFICATION

Since the signal electrons are produced away from the beam interaction point, most of them are reconstructed by the standard DØ reconstruction software as photons. Moreover, to suppress huge background from Drell-Yan, we have to require that there is no track pointing to the calorimeter cluster. To avoid confusion in terms we will call signal electrons "non-pointing electrons (NPE)", as opposed to "electrons" which are calorimeter clusters passing the shape and isolation requirements with associated track, and "photons" which are calorimeter clusters satisfying the shape and isolation criteria and have no associated track. NPE's will look exactly like photons, except that their longitudinal shower development and, therefore, efficiency to reconstruct a CPS cluster, will be similar to that of electrons. NPE's, electrons and photons will be collectively referred to as "EM objects".

We used the standard photon identification requirements in the calorimeter and tracker. The EM clusters are reconstructed in the central calorimeter (CC) with $|\eta| < 1.1$, at least 96% of the energy must be deposited in the EM section of the calorimeter, and the shower shape must be consistent with that expected of the photon. EM clusters are required to be isolated in the calorimeter (the ratio of the total calorimeter energy in cone of $\Delta\mathcal{R} < 0.4$ minus the energy of the cluster to the energy of the cluster must be below 7%). The scalar sum of all track's transverse momenta in an annulus of $0.05 < \Delta\mathcal{R} < 0.4$ is required to be less than 2 GeV (hollow cone track isolation requirement).

The EM cluster is considered to be an electron candidate if it has a matched central track or it has an electron-like pattern of hits in the tracker, and a photon candidate otherwise. In addition to the requirements above, we require EM objects to have a matched CPS cluster. The CPS efficiency for electrons is measured in $Z \to ee$ data to be 0.95 (per electron).

V. Z BOSON VERTEX RECONSTRUCTION

This section describes the EM pointing algorithm in the azimuthal plane and its use to reconstruct an intersection point of two EM object directions. To take full advantage of EM pointing one should attempt either 3-D vertexing or properly combine results of 2-D vertexing in the azimuthal (xy) and the longitudinal (rz) planes. As shown below, the vertex resolution in the rz plane is worse than that in the xy plane. So for this preliminary result we have only used vertexing in the xy plane, unless noted otherwise.

A. EM Pointing

The standard DØ reconstruction program runs an EM cluster pointing algorithm which is used to reconstruct the flight path of the EM particle assuming a straight trajectory. Its results are available for the two independent rz and xy fits. The pointing algorithm fits five shower measurements (one in the CPS and four in the four EM layers of

the central calorimeter) to a straight line which is assumed to be the EM object direction. The performance of EM pointing is verified using the $Z \rightarrow ee$ events.

B. Vertexing

The NPE trajectory for energies above 20 GeV, which are of interest to this analysis, is very close to a straight line. Therefore, the vertexing of two NPEs is just a solution of a simple system of two linear equations obtained from the pointing algorithm. Obviously, the solution will have large uncertainties when the discriminant of the system is small, or, equivalently, when the NPE trajectories are almost parallel. This is demonstrated in Fig. 2, where the difference between reconstructed and generated vertex position in a MC of a typical signal point ($M = 160$ GeV, $c\tau = 300$ mm), as well as the reconstructed vertex radius for all events (black points) and only for events with discriminant below 4000 cm^2 are shown.

Both lines are defined by two points. The first points on the lines 1 and 2 are denoted by $x_1^0,\ y_1^0$ and $x_2^0,\ y_2^0$, and the second points are defined relative to the first ones as $\Delta x_1,\ \Delta y_1$ and $\Delta x_2,\ \Delta y_2$:

$$\begin{aligned} y - y_1^0 &= (x - x_1^0)\frac{\Delta y_1}{\Delta x_1} \\ y - y_2^0 &= (x - x_2^0)\frac{\Delta y_2}{\Delta x_2}. \end{aligned}$$

Their intersection is therefore given by the solution of the equations

$$\begin{pmatrix} -\Delta y_1 & \Delta x_1 \\ -\Delta y_2 & \Delta x_2 \end{pmatrix} \begin{pmatrix} x \\ y \end{pmatrix} = \begin{pmatrix} y_1^0 \Delta x_1 - x_1^0 \Delta y_1 \\ y_2^0 \Delta x_2 - x_2^0 \Delta y_2 \end{pmatrix}$$

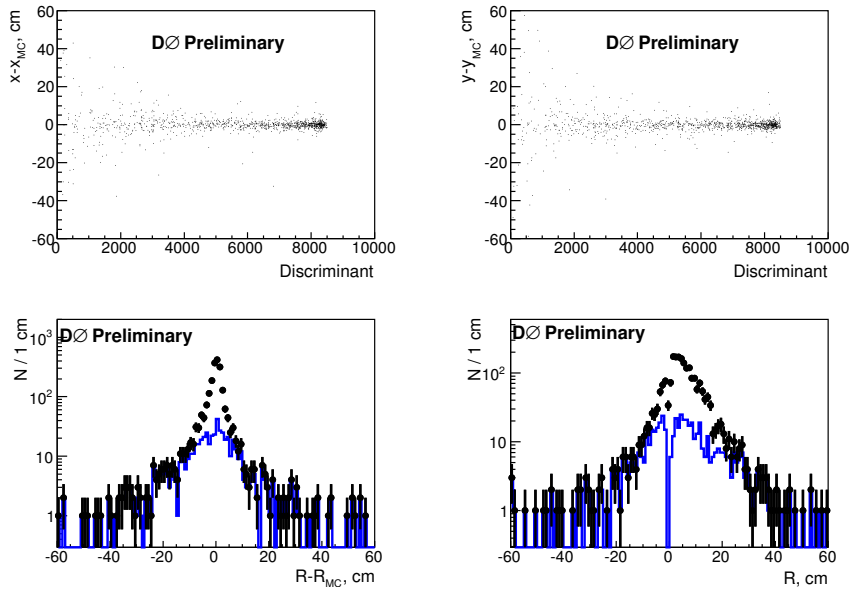

FIG. 2: Vertex reconstruction in the azimuthal plane for a typical signal point ($M = 160$ GeV, $c\tau = 300$ mm). Top plots show the difference between reconstructed and generated vertex position (x and y) *vs.* the discriminant of the system. The bottom right plot shows the reconstructed vertex radius and the bottom left plot shows the difference between the reconstructed and the generated vertex radius. Black points are all events, and blue histograms are for events with discriminant below 4000 cm^2.

Figure 4 shows the efficiency to reconstruct the vertex for events where both NPE's are reconstructed in the calorimeter and pass all selection requirements except the existence of the matching CPS cluster. Black filled circles show the probability to have CPS clusters from both NPE's reconstructed and matched. Open blued circles show efficiency of passing the cut on the discriminant.

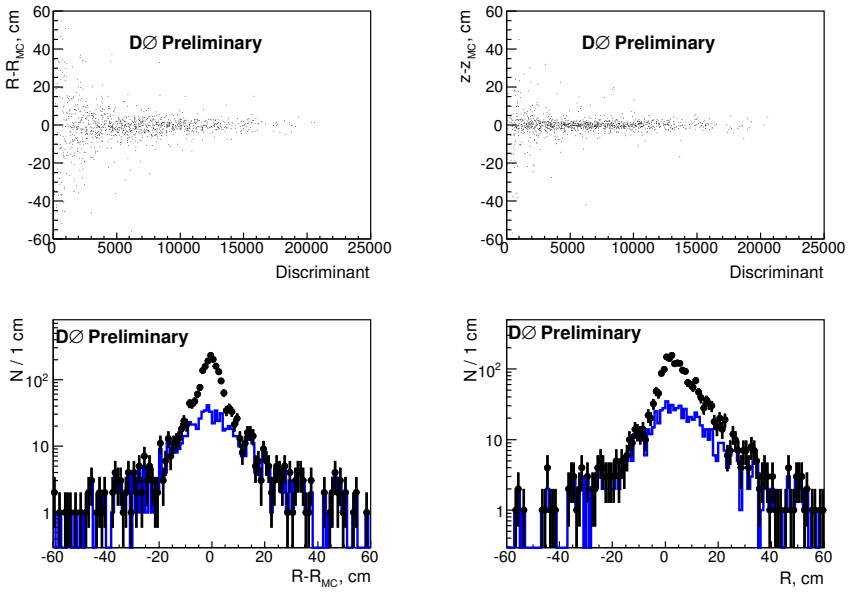

FIG. 3: Same as Fig. 2 but in rz plane. Top plots show the difference between reconstructed and generated vertex position (r and z) *vs*. the discriminant of the system. The bottom right plot shows the reconstructed vertex radius and the bottom left plot shows the difference between reconstructed and generated vertex radius. Black points are all events, and blue histograms are for events with discriminant below 4000 cm^2.

Similar vertex finding can be done in rz plane, as shown in Fig. 3, although the precision obtained is smaller. For events where both xy and rz discriminants are large, the vertex radii determined from both fits agree well with each other (see Fig. 5).

C. Sign of Vertex Radius

Vertex radius is defined as positive if the scalar vector product of the $\vec{p}_T$ of the pair of the EM objects with $\vec{r}_{vtx}$ (which is defined as a vector originating at the primary vertex and pointing to the vertex) is positive and negative otherwise. For vertices that originate from real particle decays the vertex radius should be positive within the measurement errors. We expect that the vertex radius distribution for electron or photon pairs that originate from the interaction point is symmetrical around zero. Therefore, we construct the background for positive vertex radii by mirroring the negative vertex radius distribution. Fig. 6 shows the reconstructed vertex radius for all events and for events with discriminant greater than 4000 cm^2. The blue histogram is symmetrical around zero and follows the negative part of the radius distribution.

D. Vertex Mass

As calorimeters only measure the energy of the EM objects, the invariant mass of the pair depends on the production vertex. To properly reconstruct the invariant mass we use the reconstructed position of the Z candidate vertex. For x and y of the vertex we use the xy vertex solution and for z - the rz vertex solution.

VI. DATA SAMPLE

The data were selected as in Ref. [10] using single EM triggers that are more than 99% efficient to select the signal. The total integrated luminosity of the sample [11] is 1100 ± 70 pb^{-1}.

We have selected events with two central photon candidates with $E_T > 20$ GeV as described in section IV (**signal sample**). The signal MC shows that a small fraction of the signal events do not have a primary vertex reconstructed,

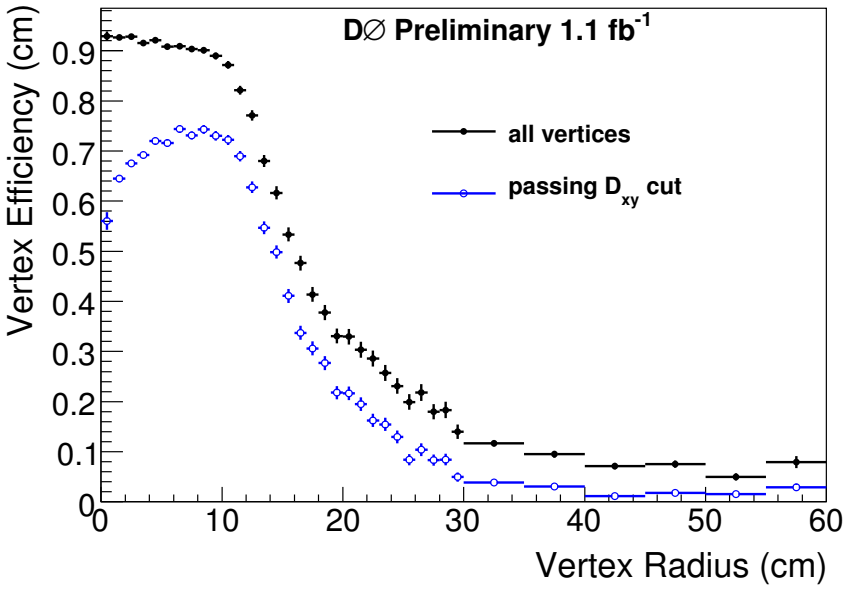

FIG. 4: Efficiency to reconstruct the vertex in the xy plane for events where both NPE's are reconstructed in the calorimeter and pass all selection requirements except the existence of the matching CPS cluster. Black filled circles show the probability to have CPS clusters from both NPE's reconstructed and matched. Open blued circles show efficiency of passing the cut on the discriminant.

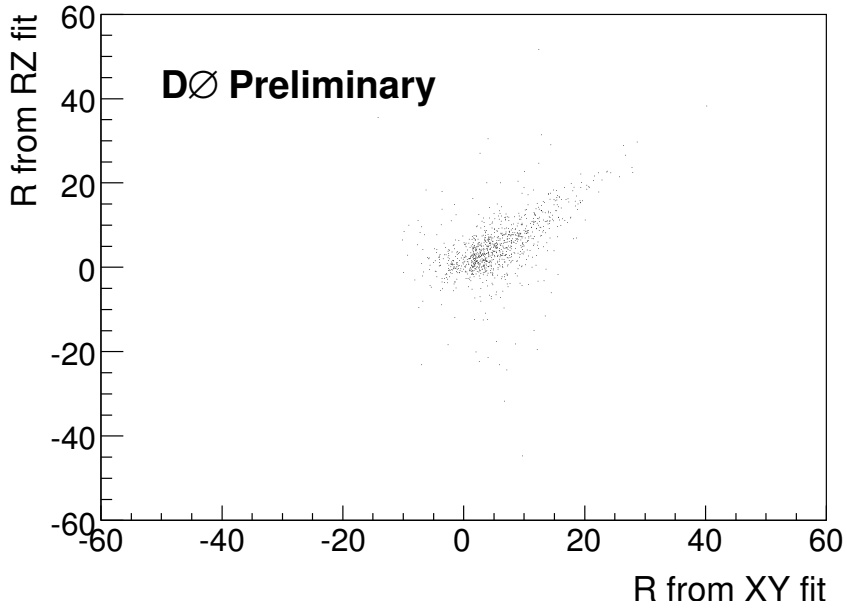

FIG. 5: Comparison of the reconstructed vertex radius in rz plane $vs.$ xy plane.

so we make no requirements on existence or position of the primary vertex.

We also selected two control samples using the same requirements except the following. The Z **sample** was obtained by requiring both EM objects to have a matched track, and the **fake sample** required that the hollow cone track isolation exceeded 4 GeV.

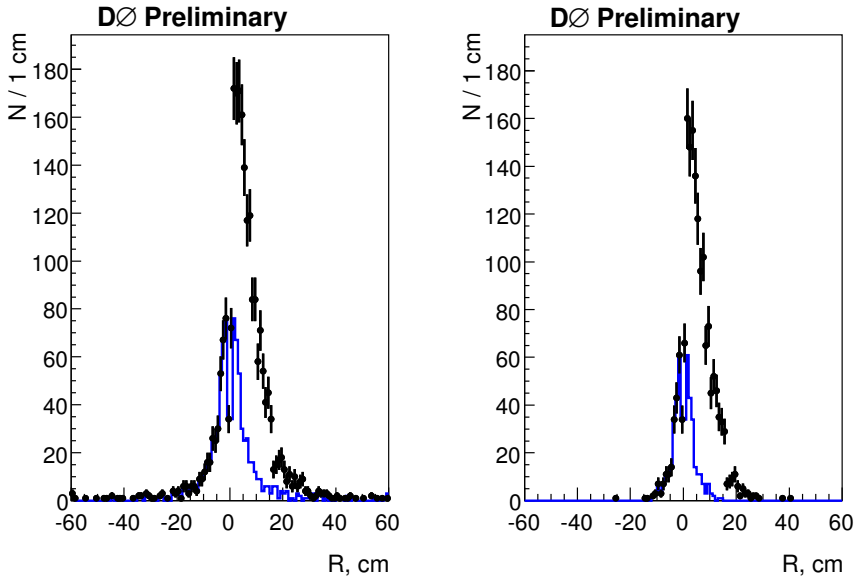

FIG. 6: Reconstructed vertex radius (in xy plane) for all events in the signal sample (left) and for events with the discriminant greater than 4000 cm^2 (right). The blue histogram is symmetrical around zero and follows the negative part of the radius distribution.

VII. DATA ANALYSIS

First, we confirm the hypothesis that the vertex radius distribution for EM objects originating from the PV is symmetrical around zero. Fig. 7 displays the reconstructed vertex radius distributions for the Z and fake samples.

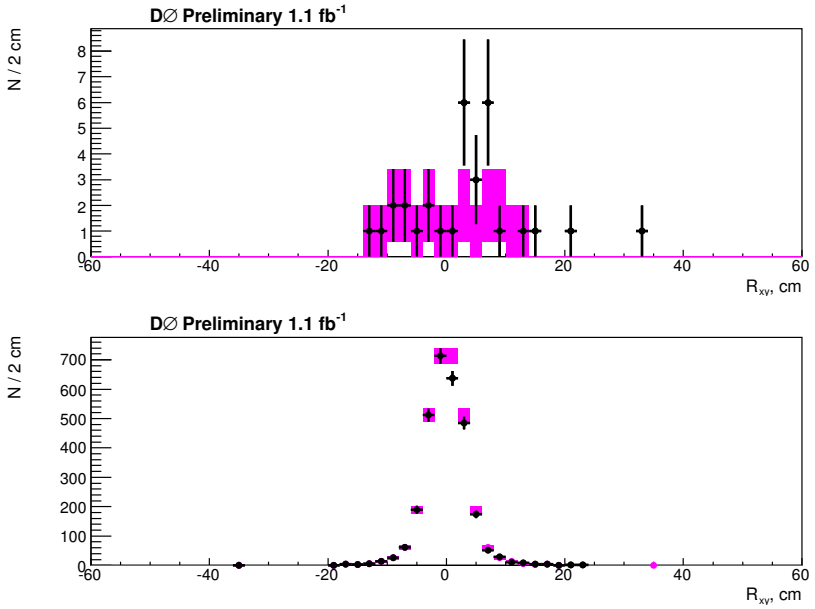

FIG. 7: Reconstructed vertex radius for the fake sample (top) and the Z sample (bottom) for vertex masses above 80 GeV. The purple histograms are mirror images of the negative parts of the distributions.

Given the positive outcome of the cross-check above, we proceed to examine the signal region. The vertex radius distributions for the vertices with mass above 75 GeV are shown in Figs. 10 and 11.

We also investigated the correlation between the discriminant of the vertex equation and the transverse momentum of the pair of EM objects. The discriminant is proportional to sine of the angle between the lines, and so is very strongly correlated with the opening angle between electrons from the Z sample which in turn is strongly correlated with Z boson's transverse momentum p_T. Fig. 8 shows the effect of the cut on discriminant on the data in the Z sample. Fig. 9 shows the effect of the cut on discriminant on reconstructed p_T of the NPE pair. Note, that unlike the Z sample, some events with large p_T are removed. This is explained by the fact that Z boson can be produced far from the primary vertex but still decay into back-to-back electrons: the discriminant in this case will be small, while the reconstructed p_T of the pair can be large.

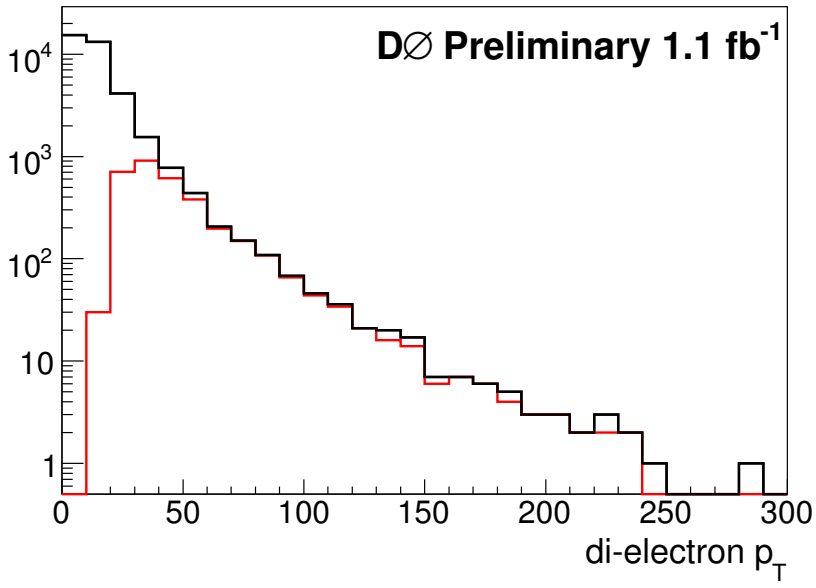

FIG. 8: Reconstructed p_T of the pair of EM objects in the Z sample for all events (black histogram) and for ones passing the cut $|d_{xy}| > 4000$ (red histogram).

Since we see no excess of events with positive vertex radius, we proceed to set limits.

VIII. LIMITS

Limits were set by fitting the data in Fig. 11 using the CL_s method with a log-likelihood ratio (LLR) test statistic [12]. The value of CL_s is defined as $CL_s = CL_{s+b}/CL_b$, where CL_{s+b} and CL_b are the confidence levels for the signal plus background hypothesis and the background-only (null) hypothesis, respectively. These confidence levels are evaluated by integrating corresponding LLR distributions populated by simulating outcomes via Poisson statistics. Systematic uncertainties are treated as uncertainties on the expected numbers of signal and background events, not the outcomes of the limit calculations. This approach ensures that the uncertainties and their correlations are propagated to the outcome with their proper weights. The systematic uncertainties for signal are dominated by signal reconstruction efficiency (15%) and luminosity (6.5%). The largest uncertainty on background prediction comes from statistical errors on the number of vertices with negative radii. We compare the observed 95% confidence level (CL) limits to LO PYTHIA cross-section for signal and obtain the 95% CL exclusion contour in mass *vs* lifetime plane shown in Fig. 12. The same in the log scale is displayed in Fig. 13.

Numerical values of the lower and upper 95% C.L. limits on $c\tau$ are given in Table II.

IX. SUMMARY

We have presented results of a search for long-lived particles that decay into a Z boson (or any final state with a pair of electrons or photons with mass above 75 GeV). We see no excess of events at positive decay lengths and

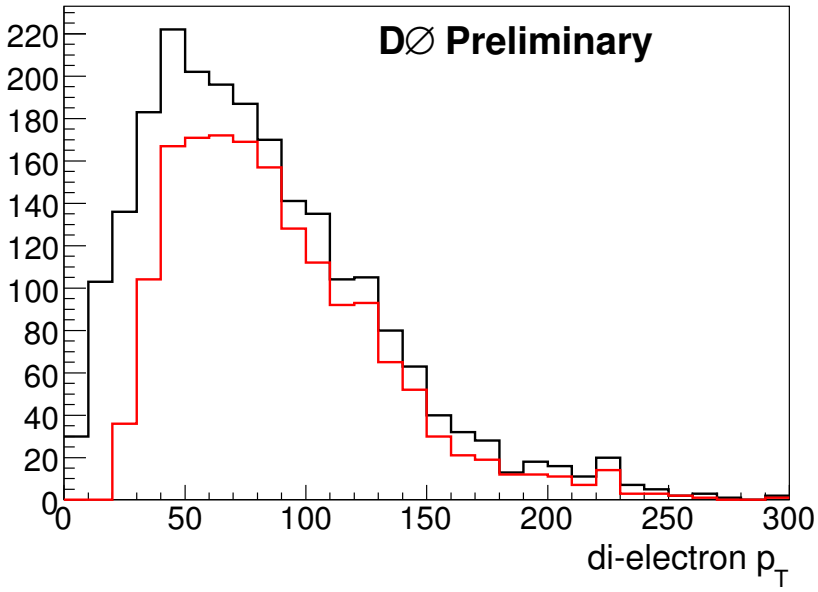

FIG. 9: Reconstructed p_T of the pair of EM objects for a signal point (160 GeV, 300 mm) for all events (black histogram) and for those passing the requirement $|d_{xy}| > 4000$ (red histogram).

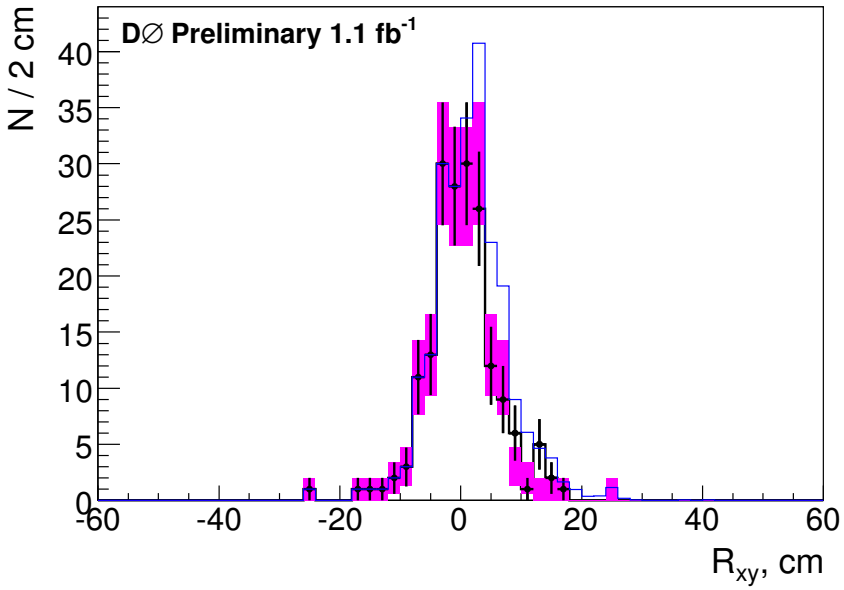

FIG. 10: Vertex radius distribution for events in the signal sample with mass greater than 75 GeV. Points with errors are data, purple histogram is a reflection of the negative part of the distribution, and the blue line correspond to an expected signal with b' mass of 160 GeV and $c\tau$ equal to 300 mm.

interpret it as a limit on the lifetime and mass of the fourth generation b'.

[1] P. Fayet, Phys. Lett. B **70**, 461 (1977); *ibid.* **86**, 272 (1979); *ibid.* **175**, 471 (1986).

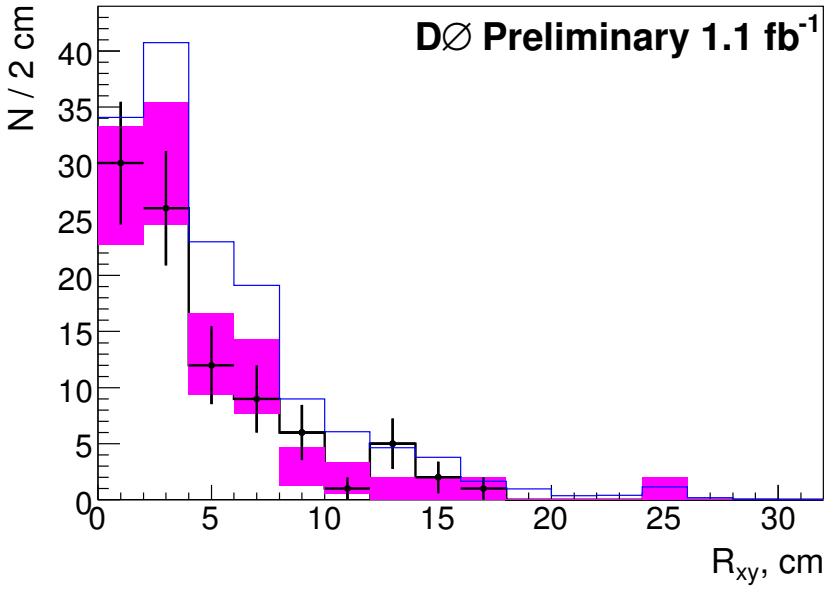

FIG. 11: Zoom into the positive side of Fig. 10.

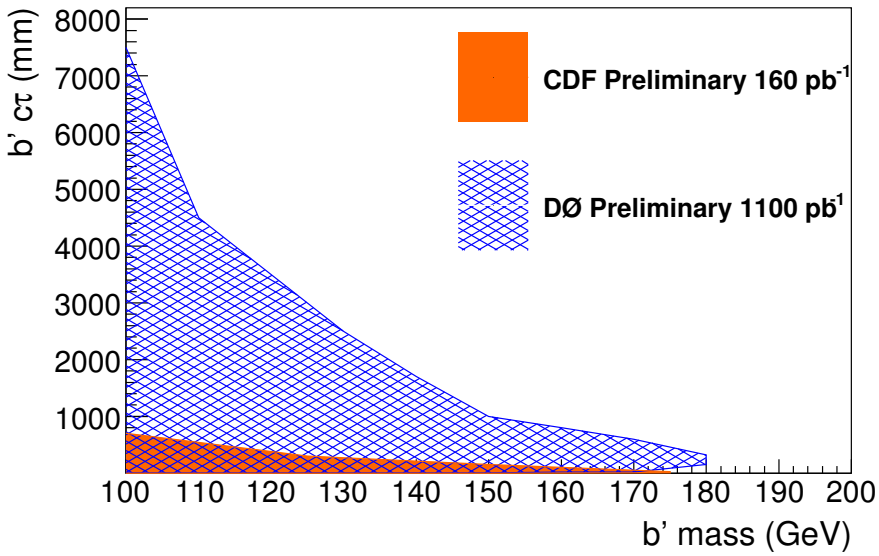

FIG. 12: The 95% C.L. exclusion limits on the b' lifetime *vs*. its mass (blue-shaded area). The CDF result is illustrated as the orange shaded contour.

[2] M. Dine, A. E. Nelson, Y. Nir and Y. Shirman, Phys. Rev. D **53**, 2658 (1996); H. Baer, M. Brhlik, C. H. Chen and X. Tata, Phys. Rev. D **55**, 4463 (1997); H. Baer, P. G. Mercadante, X. Tata and Y. L. Wang, Phys. Rev. D **60**, 055001 (1999); S. Dimopoulos, S. Thomas and J. D. Wells, Nucl. Phys. B **488**, 39 (1997); J. R. Ellis, J. L. Lopez and D. V. Nanopoulos, Phys. Lett. B **394**, 354 (1997);
see also a review by G. F. Giudice and R. Rattazzi, "Gauge-Mediated Supersymmetry Breaking" in G. L. Kane: *Perspectives on Supersymmetry*, World Scientific, Singapore (1998), p. 355-377, and references therein.

[3] M. Strassler and K. Zurek, arXiv:hep-ph/0604261v2.

[4] B. Dobrescu, G. Landsberg, K .Matchev, Phys. Rev D **63**, 075003 (2001).

[5] H. Frampton, P. Q. Hung, M. Sher, Phys. Rept. **330** 263 (2000).

[6] CDF Note 7244 `ttp://www-cdf.fnal.gov/pysics/exotic/r2a/20040826.mumulxy_longlifez/`.

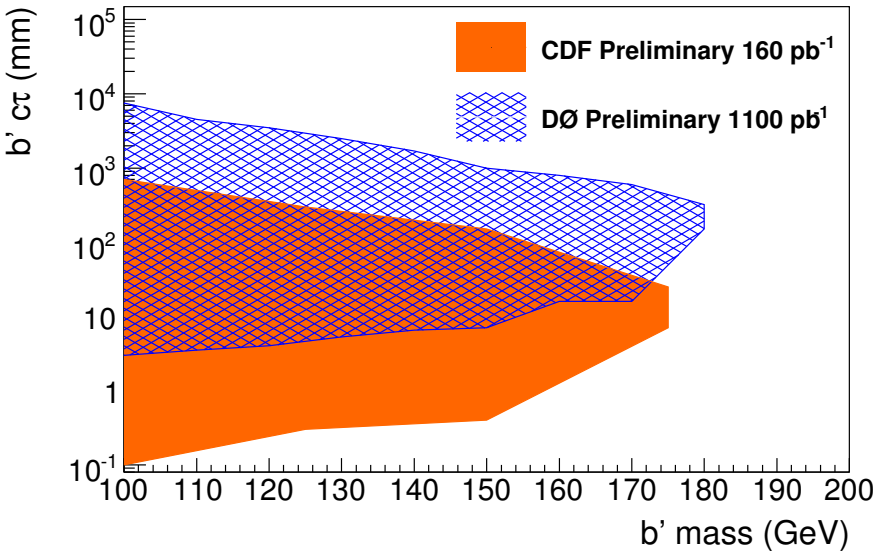

FIG. 13: The 95% C.L. exclusion limits (in log scale) on the b' lifetime *vs*. its mass (blue-shaded area). The CDF result is illustrated as the orange shaded contour.

b' mass, GeV	Lower limit on $c\tau$, mm	Upper limit on $c\tau$, mm
100	3.2	7000
110	3.8	4600
120	4.2	3500
130	5.8	2100
140	6.7	1640
150	7	900
160	16	700
170	16	530
180	160	315

TABLE II: Lower and upper 95% C.L. limits on $c\tau$ of b' as a function of the b' mass.

[7] V.M. Abazov *et al.* (D0 Collaboration), "The upgraded DØ detector," Nucl. Instrum. Methods Phys. Res. A **565**, 463 (2006).
[8] S. Abachi, *et al.* (D0 Collaboration), Nucl. Instrum. Methods Phys. Res. A **338**, 185 (1994).
[9] http://www.thep.lu.se/tf2/staff/torbjorn/Pythia.html.
[10] DØ Note 5427 `ttp://www-d0.fnal.gov/Run2Pysics/WWW/results/prelim/NP/N54/`.
[11] T. Andeen *et. al.*, FERMILAB-TM-2365-E (2006).
[12] W. Fisher, FERMILAB-TM-2386-E; T. Junk, Nucl. Instrum. Meth. A **434**, 435-443 (1999); A. Read, "Modified Frequentist Analysis of Search Results (The CLs Method)", CERN 2000-005 (30 May 2000).